Theme V – Models and Techniques for Analyzing Seismicity

Seismicity Models Based on Coulomb Stress Calculations

Sebastian Hainzl[1] • Sandy Steacy[2] • David Marsan[3]

1. Institute of Geosciences, University of Potsdam
2. School of Environmental Sciences, University of Ulster
3. Institut des Sciences de la Terre, CNRS, Universite de Savoie

Contents

Abstract Our fundamental, physical, understanding of earthquake generation is that stress-build-up leads to earthquakes within the brittle crust rupturing mainly pre-existing crustal faults. While absolute stresses are difficult to estimate, the stress changes induced by earthquakes can be calculated, and these have been shown to effect the location and timing of subsequent events. Furthermore, constitutive laws derived from laboratory experiments can be used to model the earthquake nucleation on faults and their rupture propagation. Exploiting this physical knowledge quantitative seismicity models have been built. In this article, we discuss the spatiotemporal seismicity model based on the rate-and-state dependent frictional response of fault populations introduced by *Dieterich* (1994). This model has been shown to explain a variety of observations, e.g. the Omori-Utsu law for aftershocks. We focus on the following issues: (i) necessary input information; (ii) model implementation; (iii) data-driven parameter estimation and (iv) consideration of the involved epistemic and aleatoric uncertainties.

1 Motivation

The past 20 years or so have seen a growing recognition that stress changes resulting from earthquake slip strongly affect the location and timing and subsequent events. Although a relationship between these static stress changes and the spatial distribution of aftershocks was first proposed by *Das and Scholz* (1981), the paper by *Stein et al.* (1992) following the 1992 M7.3 Landers earthquake brought this relation to the attention of the wider community. In that work, the authors demonstrated that smaller events over the preceding 17 years had increased stress at the Landers epicenter and along much of its rupture length, and that the majority of aftershocks occurred in regions where the stress had increased. Since then, numerous studies have found good qualitative agreement between static stress changes and the locations of subsequent events, both aftershocks and mainshocks (c.f. the review articles of *Harris* (1998), *Steacy et al.* (2005a), and *King* (2007))

These so-called Coulomb stress changes are computed from knowledge of the slip of the causative earthquake. The basic idea is that displacement in the elastic upper crust produces a tensorial stress perturbation which can then be resolved into shear and normal components on target (or receiver) faults; an increase in shear stress in the slip direction and a decrease in normal stress increase the likelihood of future failure (Sections 4.1.1 and 4.1.2). An example of a Coulomb stress map is shown in Figure 1, the red areas are where stress is increased, the blue where it is decreased, and the white symbols represent aftershock locations. By inspection, most but not all aftershocks occur in areas of stress increase.

Coulomb stress changes have also been shown to affect the location of subsequent mainshocks. In Turkey, for example, *Stein et al.* (1997) and *Nalbant et al.* (1998)

independently identified a portion of the North Anatolian Fault that had experienced positive Coulomb stress changes and hence was likely to be at higher risk a near-future earthquake; the M7.4 Izmit earthquake occurred on that section of the fault in 1999. More recently, *McCloskey et al.* (2005) suggested that the 2004 Sumatra earthquake had increased the likelihood of a subsequent event immediately to the south, an M8.7 earthquake occurred in that region in March, 2005. While such qualitative analyses are useful for identifying at risk areas, the real challenge is to move to the computation of changes in earthquake probabilities. The most straightforward method for this is through the rate-state formulation of *Dieterich* (1994) (see Section 4.4) and, indeed, *Parsons et al.* (2000) used this technique to estimate the increase in probability of a large earthquake in the Instanbul area resulting from the Izmit event.

Although the main focus of this article is on the typical example of static coseismic stress, and associated probability, changes, time dependent effects may also be important. In particular, viscoelastic relaxation of the lower crust (*Freed and Lin* 2002) and afterslip on the causitive fault plane (*Chan and Stein* 2009) can modify the stress field on timescales of days to years. As discussed briefly in this article, those postseismic stress changes can also be transformed in probability changes within the same framework. Additionally, the role of dynamic stress perturbations in earthquake triggering is controversial and not well understood. Previous studies demonstrated that seismic waves can trigger aftershocks, particularly in geothermal fields (*Hill et al.* 1993; *Brodsky* 2006), but it remains controversial whether dynamic triggering alone can explain the extended duration of aftershock sequences (*Belardinelli et al.* 2003; *Felzer and Brodsky* 2006). A review of this discussion is beyond the scope of this article.

2 Starting Point

Stress-based seismicity models need additional input data compared to purely statistical seismicity models which are described in the CORSSA article by Zhuang et al. They are based on physical, sound considerations and some of the parameters can be, in principal, constrained without fitting to earthquake catalog data. However, catalog data provide important constraints which should be used in practice (see Sec. 5.3). Apart from the catalog data, stress-based seismicity models need additional input informations to calculate earthquake-induced stress changes; in particular, models of mainshock slip, crustal rheology and fracture initiation. While crustal rheology models exist for most of the regions, slip models are not generally available immediately although, in the recent years, they have become more frequently and rapidly accessible, especially for large, destructive earthquakes. For instance, the National Earthquake Information Center often posts preliminary slip models within
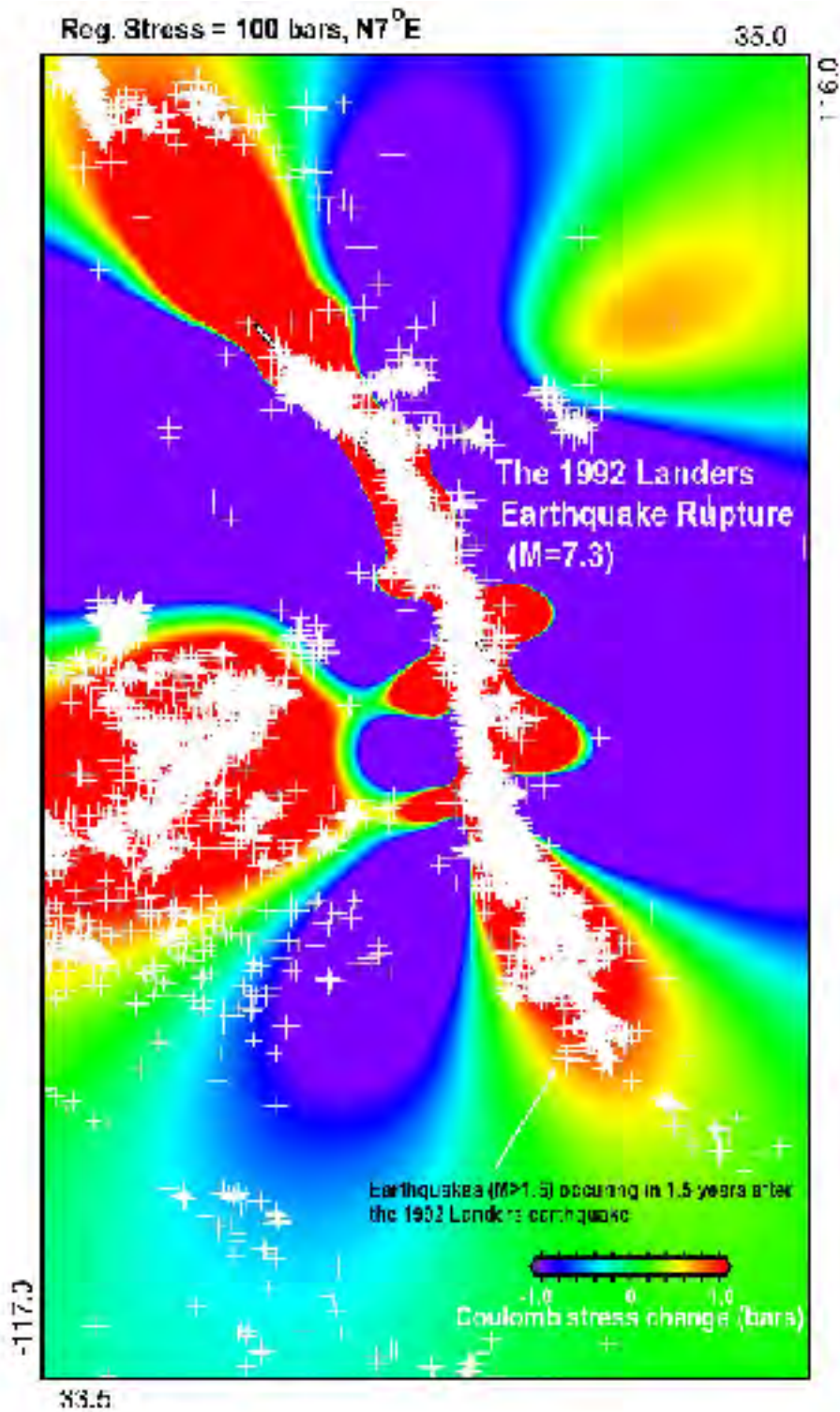
Fig. 1 Coulomb stress map for Landers earthquake. Computation based on slip model of *Wald and Heaton* (1994) and stress is resolved onto vertical optimally oriented planes.

a few hours of the occurrence of large events. For retrospective studies, a valuable resource is the finite-source rupture model database.

The first part of this article summarizes the calculation of Coulomb stress changes and introduces the seismicity model based on rate-and-state dependent friction. This part can be read without knowing the other CORSSA articles. However, later parts refer to spatiotemporal characteristics of seismicity such as the Omori-Utsu law, fitting of spatial earthquake distributions, declustering as well as to the maximum likelihood method for parameter estimation. This makes it advisable to read the corresponding CORSSA articles first.

3 Ending Point

The goal of this article is to

− clarify the underlying assumptions and input parameters of the stress-based seis-micity model
− describe the model implementation and algorithm
− provide methods for parameter estimation
− account for model uncertainties and describe their impact on the predicted stress and seismicity changes

In particular, we focus on the popular rate-and-state friction model as it has been introduced by *Dieterich* (1994). It is important to note that the purpose of this article is to discuss the technical aspects of the model implementation and application rather than to evaluate the general validity of the model.

4 Theory

4.1 Basics about Coulomb-Failure Stress calculations

In this section, we give a short overview about the theory of Coulomb-Failure stress calculations. In particular, we clarify the necessary input informations with their uncertainties. More detailed descriptions and background informations can be found in the literature, e.g. in the review articles of *Harris* (1998), *Steacy et al.* (2005a), and *King* (2007).

4.1.1 Definition

For a given fault plane and slip vector, stress changes can be quantified by changes of the Coulomb Failure Function ΔCFF which are given by

$$\Delta CFF = \Delta\tau + \mu\left(\Delta\sigma_n + \Delta p\right) \tag{1}$$

where $\Delta\tau$ is the shear stress in the direction of slip, $\Delta\sigma_n$ is the normal stress changes (positive for unclamping or extension), μ is the friction coefficient and Δp is the pore pressure change (*Harris* 1998; *King and Cocco* 2001; *Cocco et al.* 2010). The relation used to compute the coseismic pore pressure changes distinguishes the constant apparent friction model from the isotropic poroelastic model (*Cocco and Rice* 2002). According to the former model, pore pressure changes depend on the normal stress changes $\Delta p = -B\Delta\sigma_n$, where B is the Skempton coefficient which varies between 0 and 1 (*Beeler et al.* 2000; *Cocco and Rice* 2002). Therefore, using this model, equation (1) can be written as

$$\Delta CFF = \Delta\tau + \mu' \; \Delta\sigma_n \tag{2}$$

where $\mu' = \mu(1-B)$ is usually called the effective friction coefficient. On the contrary, the isotropic poroelastic model assumes that pore pressure changes depend on the volumetric stress changes (first invariant of the stress perturbation tensor) $\Delta p = -B(\Delta\sigma_{kk}/3)$, and therefore equation (1) becomes:

$$\Delta CFF = \Delta\tau + \mu \; (\Delta\sigma_n - B\frac{\Delta\sigma_{kk}}{3}). \tag{3}$$

Although both equations (2) and (3) theoretically require that the values of the friction and the Skempton coefficient are known in order to compute stress perturbations, in practice equation 2 is often used with an assumed value, such as 0.4, for the effective coefficient of friction (*King et al.* 1994; *Nalbant et al.* 2002). The uncertainty of this parameter is one source of variability in the calculation of cosesimic static stress changes and *Beeler et al.* (2000) recommend using equation (3) because it is more general and applicable to different tectonic areas. A useful discussion of the difficulties in distinguishing between these two models in realistic complex fault zones with inelastic or anisotropic properties can be found in *Cocco and Rice* (2002).

4.1.2 Input information and their related uncertainties

All applications of the stress-triggering model rely on the correct determination of the relevant stress changes. However, the stress calculation consists of unsolved problems which lead to large uncertainties such as: (i) the unknown distribution of receiver faults (*McCloskey et al.* 2003; *Steacy et al.* 2005b); (ii) the non-unique inversion results for the slip-models and mainshock fault geometry and extent (*Steacy et al.* 2004); (iii) uncalculable small scale slip variability which can lead to strong stress heterogeneities close to the source fault (*Marsan* 2006; *Hainzl and Marsan* 2008), and (iv) spatial inhomogeneity of material and pre-stress conditions.

Receiver orientation: The calculation of Coulomb stress changes requires the definition of the geometry and the faulting mechanism of the target faults upon which stress perturbations are resolved. Two approaches are commonly adopted; the first one relies on resolving stress changes onto a prescribed faulting mechanism (that is, to assign strike, dip and rake angles of the target faults). This means that fault geometry and slip direction are input parameters of stress interaction simulations. Well documented faults can be studied individually, but the stress field is then only resolved on a limited, sparse number of structures, hence possibly ignoring unknown (blind) faults that could represent a significant threat. *McCloskey et al.* (2003) proposed using geological constraints in order to calculate Coulomb stress perturbations for forecasting the spatial pattern of seismicity. However, this strategy does not always seem to be applicable, due to the complexity of fault systems for instance, as pointed out by *Nostro et al.* (2005) in their application to the 1997 Umbria-Marche (Italy) seismic sequence. The second approach relies on the calculation of the optimally oriented planes for Coulomb failure (often called OOPs). In this case, instead of assigning the strike, dip and rake angles of the receiver faults, we have to assign the magnitude and the orientation of the principal axes of the regional stress field σ_{ij}^r (*King and Cocco* 2001). The optimally oriented planes are identified at each grid point of the numerical computation by finding the values of strike, dip and rake that maximize the total stress tensor defined as $\sigma_{ij}^{tot} = \sigma_{ij}^r + \Delta\sigma_{ij}$, where $\Delta\sigma_{ij}$ is the coseismic stress perturbation. After assigning the absolute values of the principal stress components and the orientation of the stress tensor (trend and plunge of each axis), two equivalent OOPs are obtained at each node of the 3D grid.

The OOPs strongly depend on the orientation and magnitude of the regional stress field. In the far field of the stress-source, these planes are optimally oriented to the background/tectonic stress and thus in principle are closely aligned to the overall geologic features. However, in the near field, the orientation of these planes typically deviate significantly from this regional trend. In certain cases, such OOPs can be oriented such that they would be unloaded by tectonic loading. Therefore, Coulomb stress changes computed for OOPs can be associated with theoretical focal mechanisms which might not exist in reality. Moreover, as will be discussed below, the near field stress is very sensitive to unresolved details of the mainshock slip, and OOP geometry is therefore not reliable close to the main rupture.

Within even small crustal volumes, a great variety of seismogenic structures with different geometries can be potentially perturbed by the mainshock. It is thus desirable to account for more than just one target fault geometry at any given location. *Hainzl et al.* (2010) addressed this problem and proposed to evaluate the stress-based seismicity models not for a single receiver mechanism but for a whole distribution of pre-existing planes for which the slip direction is in the direction of the maximum tectonic shear stress. In practice, the considered fault distribution should be thereby

estimated, if possible, from the distribution of mapped faults in the region under consideration.

Thus, the choice of receiver fault orientation is another source of uncertainly in computing Coulomb stress perturbations, particularly near the mainshock fault.

Slip distribution: Inversions of slip distributions which are obtained from seismologic and geodetic measurements of the coseismic ground motion are usually not well constrained. As recently demonstrated by a blind test (see http://www.seismo.ethz.ch/staff/martin/BlindTest.html), slip models are often ambiguous and can significantly differ in their results even for idealized data sets, depending on the inversion strategy. The uncertainties of the slip distribution can also be seen by comparing the different solutions for the same earthquakes (see e.g., finite-source rupture model database). As an example, *Hainzl et al.* (2009) showed that the standard deviations of the stress values calculated for the 5 slip models of the 1992 M7.3 Landers mainshock are of the same order as the average stress value, hence the relative uncertaintyis almost 100%.

Furthermore, inverted slip distributions cannot resolve the small-scale slip variability. Slip inversions often show very heterogeneous slip patterns down to the scale which can still be resolved (typically a few kms) which suggests that slip might be scale-invariant (*Andrews* 1980; *Frankel* 1991; *Herrero and Bernard* 1994; *Mai and Beroza* 2002). For a two-dimensional fractal model, the slip $u(k)$ is proportional to $k^{-1-H}g(k)$ with H the Hurst exponent related to the fractal dimension $D = 3 - H$, g a realization of a Gaussian white noise, and k the wave number. In their extended analysis of the slip distributions of 44 earthquakes, *Mai and Beroza* (2002) found that $H = 0.71 \pm 0.23$. Other studies (*Lavallee et al.* 2006; *Lavallee* 2008) suggest that the slip is better modeled by a Levy, rather than Gaussian, noise g, resulting in even greater variability. As discussed in Sec. 5.3.2, the consideration of the small scale variability that is not accessible to direct measurement can explain on- and near-fault aftershock activation, even though a seismic quiescence would be otherwise expected if coarse-grained slip models were used instead.

Crustal structure: Finally, the crustal heterogeneity is not known in detail. For elastic stress-calculations, the velocity and density structure of the crust has to be specified. In the case of viscoelastic and poroelastic deformations, additional parameters such as viscosities and hydraulic diffusivities have to be assumed. Because all of these parameters are difficult to constrain by observations, the setting of the crustal model leads to further uncertainties in the stress calculations.

Furthermore, Coulomb stress changes depend on the *a priori* input parameters of the friction and the Skempton coefficients (see Sec. 4.1.1). According to several authors (*Harris* 1998; *King and Cocco* 2001; *Catalli et al.* 2008) the effect of the

friction coefficient on the stress perturbation and the seismicity rate change patterns is usually modest. On the contrary, the choice of the poroelastic model can be of relevance for computing Coulomb stress changes.

To our knowledge, a comprehensive sensitivity study of the uncertainties of Coulomb stress calculations with a disaggregation of the impact of each source has not been performed so far. Such an analysis, which would clarify the relative impact of the uncertainty and natural variability of receiver fault orientations, earthquake slip, as well as (inhomogeneous) pre-stress and crustal structure, would be very helpful and should be performed at least for some scenario events in the future.

4.2 How many mainshocks should be considered?

When modeling aftershock sequences with stress changes, it is customary to only consider the stress brought by the mainshock itself, which is generally the largest earthquake in the dataset. However, aftershocks, or even preshocks, alter the stress field as well. A well known example is provided by the Landers sequence: it is necessary to consider the M6.4 Big Bear earthquake, although an aftershock of Landers, as a source of stress change, if we aim at understanding the aftershock sequence initiated by Landers. Moreover, statistical models like the ETAS model, that do not directly calculate crustal stress, have shown that aftershocks are actually likely to contribute in a major way towards sustaining the sequence, by locally triggering their own aftershocks. The question is then to know whether the stress generated by aftershocks must be considered when mapping stress changes, and what is the magnitude aftershocks must be modeled as a stress sources.

Marsan (2005), inspired by a previous work by Kagan (1994), addressed these issues in the case of the Landers sequence. The analysis showed that there exists an ambiguity when computing stress maps. Indeed, it is customary to show stress changes computed over a whole surface, at constant depth, surrounding the mainshock. If we were to include more and more stress sources, by considering more and more aftershocks as potential 'mainshocks', such a map would be only very marginally changed. The influence of, say, a $m = 3$ aftershock on the regional activity, as measured by the corresponding stress changes, is much less than the $m = 7$ mainshock; even if one considers the whole population of $m = 3$ aftershocks, their collective influence remains negligible. Visually, a stress map is stable as long as we consider the mainshock (hence the largest event, of magnitude m_{max}) and the largest aftershocks down to magnitude $m_{max} - 1.5$.

However, most of the area shown in a stress map is of very little interest, as only a small portion contains active faults or recorded aftershocks. If we instead compute the stress changes on the faults that failed during the sequence, then the conclusions are drastically changed: aftershocks then matter in the overall stress budget.

More critically, there exists no magnitude threshold that would allow ignoring the smallest earthquakes as potential sources. This results from both the Levy-stable distribution of stress changes (as already recognized by *Kagan* (1994)) created by an earthquake, and the strong spatial clustering of aftershocks. Because they happen to be close to each other, the stress changes of previous aftershocks is effectively great on the foci of subsequent aftershocks. This argument must actually be reversed: aftershocks are close to one another because previous aftershocks transfer significant stress on the surrounding faults that then fail in subsequent aftershocks. Note that the analysis of stress changes caused by potentially very small shocks, at the location of pending earthquakes, is likely to suffer from the uncertainties on hypocenter locations. A generic model that assumes a fractal distribution for these locations was studied by *Marsan* (2005), that clearly demonstrated the importance of small shocks in the stress budget. Interestingly, the absence of a lower magnitude threshold when considering the stress budget of a sequence has also been advocated by purely statistical models (*Sornette and Werner* 2005).

4.3 Spatial correlations of stress-maps with seismicity

In order to test the quality of a stress change map, comparison to seismicity data is necessary. Three main approaches have been considered: (1) Resolving stress changes onto aftershock focal mechanisms and checking whether events were encouraged or discouraged (*Anderson and Johnson* 1999; *Hardebeck et al.* 1998; *Kato* 2006; *Lasocki et al.* 2009), (2) Comparing the spatial distribution of the aftershocks to the positive stress areas for maps assuming a particular target fault orientation (*Steacy et al.* 2004), and (3) Checking whether changes in seismicity rates coherent with the proposed stress change (*Marsan and Nalbant* 2005).

In all cases, a comparison must be made between the calculated stress changes at the observed aftershocks, and a null hypothesis that consider the stress changes generated by the mainshock as having no influence on the aftershock locations and/or plane orientation. In principle, both seismicity rate increases and decreases should correlate with positive and negative stress changes, respectively. However, seismicity shadows have been shown to be relatively rare (*Parsons* 2002; *Marsan* 2003; *Felzer and Brodsky* 2005; *Mallmann and Zoback* 2007). This observational bias towards seismicity increases will thus generally favor stress maps that mostly predict positive stress changes, as is for example the case when considering OOPs and a weak regional stress. However, as discussed in 5.3.2, accounting for small-scale stress heterogeneity (i.e. the fact that (i) stress changes can be significantly varying over short distances, and (ii) a variety of fault planes with different orientations can co-exist in small volumes) allows to reconcile this observational bias together with the existence of stress changes that are negative when averaged over a given, large volume.

4.4 Stress-based spatiotemporal seismicity model

Tectonic earthquakes seldom, if ever, occur by the sudden appearance and prop-
agation of a new shear crack (or fault). Instead, they usually involve slip along
a pre-existing fault or plate interface. They are therefore a frictional, rather than
fracture, phenomenon (*Scholz* 1998). *Brace and Byerlee* (1966) firstly pointed out
that earthquakes must be the result of a stick-slip frictional instability where earth-
quakes are the *slip*, and interseismic periods of elastic strain accumulation are the
stick. Subsequently, a complete constitutive law for rock friction has been devel-
oped based on laboratory studies. As a result many aspects of observed earthquake
phenomena, including earthquake clustering and seismic quiescence, are explained
by the nature of the friction on faults. For review articles see *Scholz* (1998), *Stein*
(1999), and *Dieterich* (2007).

Considering of a population of faults each described by the lab-derived rate-
and state-dependent friction law, *Dieterich* (1994) derived a quantitative seismicity
model based on calculations of earthquake-induced stress changes. In the following,
we focus on this friction-based seismicity model. Rather than discussing the deriva-
tions of the model, we focus on the technical aspects, in particular the formulas,
algorithms, and parameter estimation.

4.4.1 Assumptions

The main assumptions of the model are that
- constitutive friction laws known from laboratory friction experiments can be ap-
  plied to crustal faults
- a larger number of faults/sites exist in any given crustal volume on which earth-
  quakes can nucleate independently of each other (cf *Gomberg et al.* (2005) for an
  alternative model that considers a finite population of faults)
- without any stress perturbation, the system is characterized by a constant nu-
  cleation/earthquake rate r
- the system is loaded by a constant tectonic loading rate $\dot{\tau}$ which is the same
  before and after the earthquakes (this assumption can be relaxed by considering
  arbitrary stressing histories, see Sec. 5.2)

4.4.2 State-evolution equation

Following *Dieterich* (1994) the observed seismicity rate R is the expected rate of
earthquakes in a given magnitude range. It is a function of the state variable γ,
stressing rate $\dot{\tau}$ and the background seismicity rate r (*Dieterich* 1994)

$$R = \frac{r}{\gamma \dot{\tau}}. \tag{4}$$

The evolution of the state variable is governed by

$$d\gamma = \frac{1}{A\sigma} \left[dt - \gamma dS \right].$$ (5)

where σ is the effective normal stress and A is a dimensionless fault constitutive friction parameter usually $\sim$0.01 (*Dieterich* 1994; *Dieterich et al.* 2000). S is a modified Coulomb stress which is given by (*Dieterich et al.* 2000; *Catalli et al.* 2008):

$$S = \tau + (\mu - \alpha)\, \sigma$$ (6)

with the effective normal stress $\sigma = (\sigma_n + P)$ and α is the positive non-dimensional parameter controlling the normal stress changes in the *Linker and Dieterich* (1992) constitutive law. Thus ΔS can be seen as Coulomb stress change $\Delta CFF = \Delta\tau + \mu_{eff} \cdot \Delta\sigma$ with the effective friction $\mu_{eff} = (\mu - \alpha)$. However, it should be noted that the parameter multiplying the effective normal stress changes in Eq. (6) is not equal to the true friction coefficient which has to be used to calculate the optimally oriented fault planes (OOPs, see Sec. 4.1.2).

The steady state value (i.e. for $d\gamma/dt = 0$) takes the value

$$\gamma_{ss} = \frac{1}{\dot{\tau}},$$ (7)

which according to Eq. (4) gives $R = r$. We recover that, in absence of any stress perturbation, the seismicity rate in the steady state is given by the background rate of earthquake production.

4.4.3 Single stress-steps

According to the *Dieterich* (1994) model, the seismicity rate evolution $R(t)$ caused by a single stress step ΔS (at time $t = 0$) is given by

$$R(t) = \frac{r}{1 + \left[exp\left(-\frac{\Delta S}{A\sigma} \right) - 1 \right] \cdot exp\left(-\frac{t}{t_a} \right)}.$$ (8)

with the aftershock relaxation time $t_a = A\sigma/\dot{\tau}$.

For $t \ll t_a$, the seismicity rate evolution (Eq. 8) can be approximated by

$$R(t) \approx \frac{r}{\psi - (\psi - 1) \cdot t/t_a}.$$ (9)

with $\psi = exp\left(-\frac{\Delta S}{A\sigma} \right)$. This is the Omori-Utsu law with a p-value equal to 1, the c-value is given by

$$c = \psi t_a / (1 - \psi)$$ (10)

and the productivity

$$K = rt_a / (1 - \psi) \tag{11}$$

(*Cocco et al.* 2010). This imply that not only the productivity parameter K but also the c-parameter defining the delay before the onset of the $1/t$-decay depends on the value of the stress change, ΔS, which will be strongly anisotropic and distance dependent in reality. The superposition of aftershock sequences with c-values spatially differing in this way has been shown to result in apparent $p < 1$ values (*Helmstetter and Shaw* 2006). In practice, the dependence of c on ΔS is however difficult to observe in earthquake datasets (see *Ziv et al.* (2003)).

5 Available Methods

In this section, we will firstly provide algorithms to calculate the temporal evolution of the seismicity, given the stressing history and model parameters. These algorithms can be applied in each point in space to end up with the spatiotemporal seismicity model. Secondly, we mention alternative approaches for parameter estimation including physical considerations and purely data-driven maximum likelihood methodology.

5.1 Algorithm for multiple stress-steps with constant stressing rate

Starting from the stationary background rate r, the rate after a series of stress jumps ΔS_k at time t_k $(k = 1, \ldots, K)$ can be determined by Eq.(4) with

$$\gamma(t) = \frac{1}{\dot{\tau}} + \left(\gamma_{K-1} e^{-\frac{\Delta S_K}{A\sigma}} - \frac{1}{\dot{\tau}} \right) e^{-\frac{t-t_K}{t_a}}, \tag{12}$$

where $\dot{\tau}\gamma_{K-1}$ is calculated iteratively by

$$\gamma_k = \frac{1}{\dot{\tau}} + \left(\gamma_{k-1} \ e^{-\frac{\Delta S_k}{A\sigma}} - \frac{1}{\dot{\tau}} \right) e^{-\frac{t_{k+1}-t_k}{t_a}} \tag{13}$$

starting from $\gamma_0 = 1/\dot{\tau}$.

5.2 Algorithm for arbitrary stressing histories

For an arbitrary stressing history $S(t)$, which might be the result of tectonic stressing as well as dynamic, coseismic and postseismic stress changes, the evolution of γ can be tracked by considering sufficiently small times steps leading to stress increments

of $\Delta S(t)$ during time intervals of Δt. Setting the stress-step into the center of the time bin Δt, the state variable is iterated according to

$$\gamma(t + \Delta t) = \left(\gamma(t) + \frac{\Delta t}{2A\sigma}\right) e^{-\frac{S(t+\Delta t)-S(t)}{A\sigma}} + \frac{\Delta t}{2A\sigma} \tag{14}$$

starting from the background level, that is, $\gamma(0) = 1/\dot{\tau}$.

5.3 Parameter estimation

Given the stressing history, the forecasted earthquake activity depends in principal on three model parameters:

1. background rate r
2. frictional resistance $A\sigma$
3. the tectonic loading rate $\dot{\tau}$ or, alternatively, the aftershock relaxation time $t_a = A\sigma/\dot{\tau}$

The background seismicity rate: The background seismicity rate r is an important variable in any fault population model. It is the rate of earthquake production in absence of any stress perturbation. On the one hand, the background activity is expected to be non-uniform in space because of pre-existing rheological inhomogeneities of the crust. On the other hand, it is associated with a temporally stationary process. Background events are expected to occur independently of each other (i.e., the nucleating patches do not interact), and thus the background seismicity rate can be considered as a time independent Poisson process. The background rate can be in principal estimated from the declustered catalog (see, e.g., van Stiphout et al.). However, in the case of sparse data, the estimation of the spatial distribution might be difficult in practice. (For details, see Werner et al..).

Frictional resistance $A\sigma$: This parameter is not well-constrained beforehand. While the dimensionless fault constitutive friction parameter A is approximately known from laboratory experiments; ~ 0.01 (*Dieterich* 1994; *Dieterich et al.* 2000), the absolute value of the effective normal stress σ is mostly unknown, and must a priori depend on depth, regional stress, fault orientation, and pore pressure. The value of $A\sigma$ is usually set by data fitting, and assumed to be uniform over large volumes. In previous applications of the model, $A\sigma$ has been estimated in the range between 0.01 and 0.1 MPa; e.g. $A\sigma \approx 0.02$ MPa for the 1992 $M_w 7.3$ Landers earthquake (*Hainzl et al.* 2009); $A\sigma = 0.035 \pm 0.015$ MPa for the 1995 $M_w 6.9$ Kobe earthquake (*Toda et al.* 1998; *Stein* 1999); $A\sigma = 0.01$ MPa for the 2000 Izu earthquake swarm (*Toda et al.* 2002); and $A\sigma = 0.04$ MPa for the 1997 Umbria-Marche sequence in central Italy (*Catalli et al.* 2008); and $A\sigma = 0.012$ MPa for the seismicity between 1970-2003 in Japan (*Console et al.* 2006).

Tectonic loading rate $\dot{\tau}$: The third parameter is the tectonic loading rate $\dot{\tau}$ or, alternatively, the aftershock relaxation time $t_a = A\sigma/\dot{\tau}$. The latter gives the time scale after which the aftershock activity induced by a sudden stress increase has decayed so much that it becomes almost indistinguishable from background activity.

The tectonic loading rate is not independent of the other parameters: It is correlated with the background rate because the seismic moment released by the background activity has to equal the seismic moment induced by tectonic loading in a seismically fully coupled region. Based on *Kostrov* (1974), *Catalli et al.* (2008) deduced the following linear relation between the loading $\dot{\tau}$ and the background rate r:

$$\dot{\tau} = \langle \Delta\tau \rangle \cdot r \qquad\qquad (15)$$

$$\text{with} \quad \langle \Delta\tau \rangle \equiv \frac{10^{9.1+1.5M_{min}}}{V} \frac{b}{1.5-b} \left(10^{(1.5-b)(M_{max}-M_{min})} - 1\right)$$

which is valid assuming that all earthquakes have the same mechanism and following a Gutenberg-Richter frequency-magnitude distribution (related to the b-value and a minimum and maximum magnitude, M_{min} and M_{max}). Here V is the seismogenic volume in which the seismicity rate r is computed. The unit of $\langle \Delta\tau \rangle$ is Pascal if V is given in units of m^3.

Thus, knowing the background seismicity rate and the frequency-size distribution as well as the seismogenic thickness, the tectonic loading is fixed and the rate-and-state model consists only of two independent parameters, r and $A\sigma$.

Two alternative approaches are applied to estimate these parameters: (i) curve fitting of locally observed values of the rate changes R/r and (ii) the maximum Loglikelihood method. The maximum Likelihood method has been applied recently in different applications (*Console et al.* 2006; *Catalli et al.* 2008; *Hainzl et al.* 2009) and is in detail described in the next subsection. Here, we only briefly describe the former, alternative approach which has been e.g. applied by *Toda et al.* (1998) and *Toda et al.* (2002). In this case, the local ratios of the observed (smoothed) seismicity rates before and after the mainshock R_{obs}/r_{obs} are plotted versus the calculated Coulomb stress changes ΔCFF. The data points are fitted by the model prediction which is given by the integration of Eq. (8) between 0 and the end of the observation interval T (divided by the number of background events expected in the same time interval, rT). For a given observation time T, the resulting model curve depends on the two parameters t_a and $A\sigma$. By setting $\dot{\tau}$ or t_a independently, the curve fitting can be used for the estimation of the parameter $A\sigma$.

5.3.1 Parameter estimation by maximum likelihood method

The likelihood function L is the joint probability function for a given model and can be constructed by multiplying the probability density function of each of the

data points together. For a given time interval $[t_0, t_1]$ and spatial volume $[x_0, x_1]$ x $[y_0, y_1]$ x $[z_0, z_1]$, the log-likelihood with respect to the N earthquakes that occurred at times t_n and locations $\mathbf{x}_n = [x_n, y_n, z_n]$ can be determined by

$$\ln L = \sum_{n=1}^{N} \ln R(\mathbf{x}_n, t_n) - \int\limits_{t_0}^{t_1} \int\limits_{x_0}^{x_1} \int\limits_{y_0}^{y_1} \int\limits_{z_0}^{z_1} R(x, y, z, t) \, dx \, dy \, dz \, dt \tag{16}$$

(*Ogata* 1998; *Daley and Vere-Jones* 2003).

In practice, the $\ln L$-function is calculated by discretization of the spatial volume (*Hainzl et al.* 2009). The seismogenic volume under consideration is subdivided into K sub-volumes of identical volume ΔV. The stress changes $\Delta CFF(\bar{\mathbf{x}}_k)$ are calculated at the central points $\bar{\mathbf{x}}_k$ of these sub-volumes $(k = 1, \ldots, K)$. For given parameters and stressing history, the seismicity rate evolution $R(\bar{\mathbf{x}}_k, t)$ is calculated at the grid-points by the algorithms given in sections 5.1 or 5.2. The space integrals are therefore approximated by a summation

$$\int\limits_{t_0}^{t_1} \int\limits_{x_0}^{x_1} \int\limits_{y_0}^{y_1} \int\limits_{z_0}^{z_1} R(x, y, z, t) \, dx \, dy \, dz \, dt \approx \triangle V \cdot \sum_{k=1}^{K} \int\limits_{t_0}^{t_1} R(\bar{\mathbf{x}}_k, t) dt \tag{17}$$

For the first part of the $\ln L$-calculation, the seismicity rate for each earthquake n is approximated by the seismicity rate in the closest grid point $\bar{\mathbf{x}}_n$ to this earthquake, i.e. $\ln R(\mathbf{x}_n, t_n) \approx \ln R(\bar{\mathbf{x}}_n, t_n)$, if location errors can be ignored. However, in general, location errors should be taken into account. Then the value $R(\mathbf{x}_n, t_n)$ has to be replaced by the weighted sum $\sum_{k=1}^{K} w_k R(\bar{\mathbf{x}}_k, t_n)$ where w_k is the probability that the earthquake n occurred in the sub-volume k. The weights can be calculated according to the Gaussian-distributed location errors given in the catalog.

For given parameters $A\sigma$ and t_a (or $\dot{\tau}$), the ratio R/r can be calculated because it is independent of r. Therefore, the maximization of the log-likelihood function with respect to r can be solved analytically from setting $dL/dr = 0$ leading to

$$r = N \left[\int\limits_{t_0}^{t_1} \int\limits_{x_0}^{x_1} \int\limits_{y_0}^{y_1} \int\limits_{z_0}^{z_1} \frac{R(x, y, z, t)}{r} \, dx \, dy \, dz \, dt \right]^{-1}$$

$$\approx N \left[\triangle V \cdot \sum_{k=1}^{K} \int\limits_{t_0}^{t_1} \frac{R(\bar{\mathbf{x}}_k, t)}{r} \, dt \right]^{-1} \tag{18}$$

Thus, a systematic search of the $\ln L$-maximum has to be performed only with respect to the remaining parameters $(A\sigma, t_a, \text{ or } \dot{\tau})$. This can be done, e.g., by means of a simple grid-search or other algorithms.

5.3.2 Consideration of uncertainties and intrinsic variability

As discussed in Sec. 4.1.2, stress calculations consist of large uncertainties. The confidence intervals (standard deviation) of calculated stress values are likely to be of the same order as the mean stress value at each location due to the uncertainties of the slip distributions, the receiver fault mechanisms and the crustal structure (*Hainzl et al.* 2009). Such large uncertainties cannot be ignored. Additionally to the epistemic uncertainties related to these unconstrained ingredients of the stress calculations, also aleatoric uncertainties have to be taken into account which are related to intrinsic variability of the system. Those uncertainties result from small scale variability of slip, pre-stress, and crustal properties that are not accessible to direct measurement nor deterministic computation *Marsan* (2006).

To take these uncertainties appropriately into account, the seismicity rates have to be calculated for the full distribution of possible stressing histories rather than for only one scenario. For example in the case of a single stress step, the size of the stress step is now described by a probability function $f(\Delta S)$ instead of one certain value and the old model prediction of $R(t)$ in Eq. (8) has to be replaced by

$$R(t) = \int R(t, \Delta S) \; f(\Delta S) \; d(\Delta S) \quad . \tag{19}$$

Because the probability density function $f(\Delta S)$ will be in general not known in detail, it has to be approximated. A standard choice might be the Gaussian distribution which is defined by two parameters: the mean and the standard deviation.

Helmstetter and Shaw (2006) and *Marsan* (2006) showed that the consideration of intrinsic variability by means of broad probability distributions can explain earthquake activation in regions characterized by a mean negative stress change (so-called stress shadows) immediately after the mainshock. In particular, stress field variability due to small-scale slip heterogeneity leads to aftershocks within the rupture area where seismic quiescence which would be otherwise expected if coarse-grained slip models are used only (*Marsan* 2006; *Hainzl and Marsan* 2008).

To account for the uncertainty of the stress changes, one can use Monte-Carlo simulations. In each sub-volume, Z scenarios of stressing histories $\mathbf{\Delta S} = [\Delta S_1, \ldots, \Delta S_M]$ are created where each of the M stress jumps is randomly selected from the corresponding probability distribution f. The likelihood-value L is replaced by $\langle L \rangle = (1/Z) \sum_{z=1}^{Z} L(\mathbf{\Delta S}_z)$. To guarantee a good sampling of the probability distributions, the number of Monte-Carlo simulations Z should increase with the number of stress steps M. Maximizing this revised likelihood-value $\langle L \rangle$ (or equivalently maxizing the log-likelihood value $\ln(\langle L \rangle)$) leads to a parameter estimation under consideration of the stress uncertainty/variability (*Marsan and Daniel* 2007; *Hainzl et al.* 2009).

6 Benchmarks

A full benchmark test of the model for one of the CORSSA data sets requires a number of additional data and definitions:

- slip models for all earthquakes for which stress changes should be calculated.
- choice of the receiver fault mechanisms and friction coefficient (see Sec. 4.1.2)
- definition of the spatial grid on which Coulomb stress is calculated (width of the seismogenic layer and distance between grid points)
- definition of the involved uncertainties of the stress calculation
- choice of the parameter estimation procedure: parameter setting by physical constraints or pure data fitting (Sec. 5.3)

Because there is no general consensus about these points so far, a full benchmark test for a larger data set makes no sense. Instead of performing a full test, modelers should however test their model implementation in the following two ways:

1. Test for a single stress step if the earthquake rate $R(t)$ follows the analytic solution of Eq. (8) in each grid node.
2. Perform a synthetic test for the parameter estimation: For Monte-Carlo simulations of seismicity triggered by a (synthetic or real) earthquake slip distribution, test whether the parameter estimation procedure recovers, on average, the input parameters if the same stress calculations are used for the Monte-Carlo simulations and the parameter estimation.

If these tests are successful, the model can be applied to real data. However, for applications to real data, it is important to be aware of the incompleteness of the aftershock catalogs within the first hours or days after a main shock (see Theme IV). In the first time, smaller magnitude earthquakes are only partly recorded due to the high activity level. With decreasing aftershock activity, the catalog completeness recovers again the level which it had been before the mainshock. While empirical models such as the ETAS model can adapt to it by adjust the c-value of the Omori-Utsu law, the stress-based model predicts the real number of aftershocks and cannot take incomplete recordings directly into account. Thus, in the case of the latter model, the estimation of the parameters has to be in general restricted to time intervals where the completeness is ensured. This can be simply done by ignoring the first hours/days of aftershock activity. For the same reason, it is meaningless to compare the stress-model forecasts for the first aftershocks with the observations. Tests have to be generally also restricted to later time periods with complete recordings. The model application can only be expanded to other time periods if the probability $p(m, t)$ that the seismic network could detect a magnitude m at time t is explicitly known (*Marsan and Daniel* 2007).

7 Examples of Excellent Applications in the Literature

7.1 Considering stress variability

Marsan and Daniel (2007) analyzed the aftershock activity of the 1999 $M_w7.6$ Chi-Chi, Taiwan earthquake which was characterized by the existence of several locations with delayed onset of seismic quiescence, especially off the Chelungpu fault on which the earthquake took place. The authors applied the described rate-and-state dependent friction model of *Dieterich* (1994) and analyzed whether of heterogeneous static-stress transfer can explain this observation. For that they model the distribution of coseismic small-scale stress change by a Gaussian law with mean $\overline{\Delta S}$ and standard deviation $\sigma_{\Delta S}$ where the latter measures the level of local heterogeneity of the coseismic change in stress. The model was shown to mimic the earthquake time series very well. Robust inversion of the $\overline{\Delta S}$ and $\sigma_{\Delta S}$ parameters could be achieved at various locations. The authors demonstrated that several quiescences have delays that can be well explained by local stress heterogeneity, even at relatively large distances from the Chi-Chi earthquake.

In the case of the Chi-Chi earthquake, both, the mean stress values and their corresponding standard deviations, were inverted from aftershock data in specific locations without using the additional information of the inverted mainshock slip distribution. In the case of the aftershock sequence of the 1992 M7.3 Landers mainshock, *Hainzl et al.* (2009) performed a parameter estimation (including the standard deviation of the stress values) based on the stress changes $\overline{\Delta S}$ determined from previously published slip models. The authors applied the maximum Likelihood methodology under consideration of the stress uncertainties (see Sec. 5.3.2). For that, they also assumed Gaussian distributions to describe the probability distribution of the stress values of each stress step where the mean values of the Gaussian distributions, $\overline{\Delta S_k}$, were set to the deterministically calculated stress value based on the underlying slip model and the standard deviation, $\sigma_{\Delta S,k}$, were assumed to be simply proportional to the mean values, namely $\sigma_{\Delta S,k} = C_V \cdot \overline{\Delta S_k}$, with C_V being the same for all locations. The proportional constant C_V (coefficient of variation) was itself estimated by searching the value which maximizes the likelihood-value. As a result of taking the stress uncertainty into account, the parameter estimation becomes stable and the model reproduces of the spatiotemporal aftershock occurrence very well. Thereby, the estimation of the coefficient of variation yields a value of $C_V = 0.95$ indicating that the standard deviations of the stress uncertainty/variability are close to the absolute values.

7.2 Stress inversion based on the rate-and-state friction model

The discussed rate-and-state friction model for spatiotemporal seismicity evolution cannot only be used for forward simulations in order to forecast the earthquake activity based on a given stressing history, but also to invert the stressing history giving an observed seismicity evolution. *Dieterich et al.* (2000) showed that the temporal stress evolution can be inverted by

$$\Delta S(t_n + 0.5\Delta t) = A\sigma \ln \left(\frac{\gamma(t_n) + \frac{\Delta t}{2A\sigma}}{\gamma(t_{n+1}) - \frac{\Delta t}{2A\sigma}} \right) \tag{20}$$

with $\gamma(t) = r/[R(t)\dot{\tau}]$ where the seismicity rate R is measured in time bins of Δt at time steps $t_1, t_2, \ldots t_N$. The application of this method at Kilauea volcano, in Hawaii, yields good agreement with independent estimates, indicating that earthquake rates can provide a practical remote-sensing stress meter.

7.3 Simulations of coupled fault networks

While the model is often only applied to analyze isolated clusters in space and time (aftershock sequences or swarms), the model can also be used to simulate seismicity evolution on larger spatial and temporal scales. For example, *Toda et al.* (2005) applied the algorithm for multiple stress-steps (Sec. 5.1) in order to analyze the seismicity evolution in California during the time interval between 1986 and 2003 in a 300 km times 310 km area centered on the 1992 M = 7.3 Landers earthquake. The animations show that the model simulations can reproduce much, but certainly not all, of the observed spatial and temporal seismicity. As a result of their study, the authors inferred that the decaying effect of stress transferred by successive main shocks influences seismicity for decades.

However, the seismicity model for fault populations with rate-and-state dependent friction - as discussed in previous sections - ignores the dependence of the earthquake rupture growth (magnitudes) on the stress state and might therefore result in erroneous forward simulations. For simulations of possible future scenarios of fault interactions and the recurrence of large earthquakes on specific faults, more sophisticated model implementations should be considered in general with spontaneous rate-and-state dependent frictional nucleation and growth of earthquake ruptures on discretized and interacting crustal faults. Such model implementations have been previously introduced by *Dieterich* (1995); *Ziv and Rubin* (2003); *Lapusta and Liu* (2009); *Dieterich and Richards-Dinger* (2010)

8 Summary, Further Reading, Next Steps

Deterministic Coulomb-stress calculations provide important results based on our physical process understanding. Therefore, it is desirable to use these additional deterministic information, if available, for seismicity modeling. In the past, Coulomb-stress calculations have been often shown to be very successful in describing overall features of triggered seismicity. However, even on the short time scales, purely deterministic approaches are not able to describe the details of the earthquake dynamics. One reason for this is the limited access to important state variables of the underlying processes (e.g. subsurface pre-stresses and material properties). Direct observations are only possible in a few specific locations where expensive deep holes have been drilled into the crust. Besides our epistemic uncertainties due to unconstrained stress states and crust models, aleatoric variability plays an important role. The existence of small scale stress and material heterogeneities, which will be in general not accessible to direct measurements, will preclude the possibility of purely deterministic earthquake predictions. However, although pure deterministic approaches are not applicable, our physical knowledge should not be ignored because it gives important constraints.

In order to advance in the field of earthquake forecasting, deterministic and probabilistic approaches should be combined to end up with physics-based probabilistic models. Some promising steps are already done in the context of the stress-based seismicity models (see Sec. 5.3.2). Such combinations of deterministic and probabilistic approaches should be further developed in the future to allow an adequate modeling of the time- and space-dependence of the earthquake process with its intrinsic variability.

References

Anderson, G., and H. Johnson (1999), A new statistical test for static stress triggering: Application to the 1987 Superstition Hills earthquake sequence, *J. Geophys. Res.*, *104*, 20,153–20,168. 11

Andrews, D. J. (1980), A stochastic fault model: 1. static case, *J. Geophys. Res.*, *85*, 3867–3877. 9

Beeler, N., R. W. Simpson, S. H. Hickman, and D. A. Lockner (2000), Pore fluid pressure, apparent friction, and Coulomb failure, *J. Geophys. Res.*, *105*(B11), 25,533–25,542. 7

Belardinelli, M. E., A. Bizzarri, and M. Cocco (2003), Earthquake triggering by static and dynamic stress changes, *J. Geophys. Res.*, *108*, 2135, doi:doi:10.1029/2002JB001779. 4

Brace, W. F., and J. D. Byerlee (1966), Stick slip as a mechanism for earthquakes, *Science*, *153*(990-992). 12

Brodsky, E. E. (2006), Long-range triggered earthquakes that continue after the wave train passes, *Geophys. Res. Lett.*, *33*(L15313). 4

Catalli, F., M. Cocco, R. Console, and L. Chiaraluce (2008), Modeling seismicity rate changes during the 1997 Umbria-Marche sequence (central Italy) through rate- and state-dependent model, *J. Geophys. Res.*, *113*(B11301), doi:10.1029/2007JB005356. 9, 13, 15, 16

Chan, C. H., and R. S. Stein (2009), Stress evolution following the 1999 Chi-Chi, Taiwan, earthquake: consequences for afterslip, relaxation, aftershocks and departures from Omori decay, *Geophys. J. Int.*, *177*(1), 179–192. 4

Cocco, M., and J. R. Rice (2002), Pore pressure and poroelasticity effects in Coulomb stress analysis of earthquake interactions, *J. Geophys. Res.*, *107*(B2), 2030. 7

Cocco, M., S. Hainzl, F. Catalli, B. Enescu, A. M. Lombardi, and J. Woessner (2010), Sensitivity study of forecasted aftershock seismicity based on Coulomb stress calculation and rate- and state-dependent frictional response, *J. Geophys. Res.*, *115*(B05307), doi:10.1029/2009JB006838. 7, 14

Console, R., M. Murru, and F. Catalli (2006), Physical and stochastic models of earthquake clustering, *Tectonophysics*, *417*(1-2), 141–153. 15, 16

Daley, D. J., and D. Vere-Jones (2003), *An Introduction to the Theory of Point Processes*, vol. I, Springer, New York, USA. 17

Das, S., and C. H. Scholz (1981), Off-fault aftershock clusters caused by shear-stress increase?, *Bull. Seis. Soc. Am.*, *71*, 1669–1675. 3

Dieterich, J. H. (1994), A constitutive law for rate of earthquake production and its application to earthquake clustering, *J. Geophys. Res.*, *99*, 2601–2618. 3, 4, 6, 12, 13, 15, 20

Dieterich, J. H. (1995), Earthquake simulations with time-dependent nucleation and long-range interactions, *J. Nonlinear Proc. Geophys.*, *2*, 109120. 21

Dieterich, J. H. (2007), Applications of rate- and state-dependent friction to models of fault slip and earthquake occurrence, *Treatise on Geophysics*, *4*, 107–129. 12

Dieterich, J. H., and K. B. Richards-Dinger (2010), Earthquake recurrence in simulated fault systems, *Pure Appl. Geophys.*, doi:10.1007/s00024-010-0094-0. 21

Dieterich, J. H., V. Cayol, and P. Okubo (2000), The use of earthquake rate changes as a stress meter at Kilauea volcano, *Nature*, *408*, 457. 13, 15, 21

Felzer, K. R., and E. E. Brodsky (2005), Testing the stress shadow hypothesis, *J. Geophys. Res.*, *110*, B05S09. 11

Felzer, K. R., and E. E. Brodsky (2006), Decay of aftershock density with distance indicates triggering by dynamic stress, *Nature*, *441*, 735–738. 4

Frankel, A. (1991), High-frequency spectral falloff of earthquakes, fractal dimension of complex rupture, *b* value, and the scaling of strength on fault, *J. Geophys. Res.*, *96*, 6291–6302. 9

Freed, A. M., and J. Lin (2002), Accelerated stress buildup on the southern San Andreas fault and surrounding regions caused by Mojave Desert earthquakes, *Geology*, *30*, 571–574. 4

Gomberg, J., P. Reasenberg, M. Cocco, and M. E. Belardinelli (2005), A frictional population model of seismicity rate change, *J. Geophys. Res.*, *110*(B5), B05S03. 12

Hainzl, S., and D. Marsan (2008), Dependence of the Omori-Utsu law parameters on mainshock magnitude: observations and modeling, *J. Geophys. Res.*, *113*, B10,309, doi:10.1029/2007JB005492. 7, 18

Hainzl, S., B. Enescu, M. Cocco, J. Woessner, F. Catalli, R. Wang, and F. Roth (2009), Aftershock modeling based on uncertain stress calculations, *J. Geophys. Res.*, *114*, B05,309. 9, 15, 16, 17, 18, 20

Hainzl, S., G. Zöller, and R. Wang (2010), Impact of the receiver fault distribution on aftershock activity, *J. Geophys. Res.*, *115*, B05,315, doi:doi:10.1029/2008JB006224. 8

Hardebeck, J. L., J. J. Nazareth, and E. Hauksson (1998), The static stress change triggering model: Constraints from two southern California aftershock sequences, *J. Geophys. Res.*, *103*(B10), 24,427–24,437. 11

Harris, R. A. (1998), Introduction to special section: Stress triggers, stress shadows, and implications for seismic hazard, *J. Geophys. Res.*, *103*, 24,347–24,358. 3, 6, 7, 9

Helmstetter, A., and B. E. Shaw (2006), Relation between stress heterogeneity and aftershock rate in the rate-and-state model, *J. Geophys. Res.*, *111*, B07,304. 14, 18

Herrero, A., and P. Bernard (1994), A kinematic self-similar rupture process for earthquakes, *Bull. Seis. Soc. Am.*, *84*, 1216–1288. 9

Hill, D. P., P. A. Reasenberg, A. Michael, W. J. Arabaz, G. Beroza, D. Brumbaugh, J. N. Brune, R. Castro, S. Davis, D. Depolo, W. L. Ellsworth, J. Gomberg, S. Harmsen, L. House, S. M. Jackson, M. J. S. Johnston, L. Jones, R. Keller, S. Malone, L. Munguia, S. Nava, J. C. Pechmann, A. Sanford, R. W. Simpson, R. B. Smith, M. Stark, M. Stickney, A. Vidal, S. Walter, V. Wong, and J. Zollweg (1993), Seismicity remotely triggered by the magnitude 7.3 Landers, *Science*, *260*, 1617–1623. 4

Kagan, Y. Y. (1994), Distribution of incremental static stress caused by earthquakes, *Nonl. Proc. Geophys.*, *1*, 172–181. 10, 11

Kato, M. (2006), Static Coulomb failure function and aftershocks of 1995 Kobe earthquake: A statistical test, *Geophys. Res. Lett.*, *33*, L17,313. 11

King, G. C. P. (2007), Fault interaction, earthquake stress changes, and the evolution of seismicity, *Treatise on Geophysics*, *4*, 225–255. 3, 6

King, G. C. P., and M. Cocco (2001), Fault interaction by elastic stress changes: New clues from earthquake sequences, *Advances Geophys.*, *44*, 1–38. 7, 8, 9

King, G. C. P., R. S. Stein, and J. Lin (1994), Static stress changes and the triggering of earthquakes, *Bull. Seis. Soc. Am.*, *84*, 935–953. 7

Kostrov, V. V. (1974), Seismic moment and energy of earthquakes, and seismic flow of rock, *Earth Phys.*, *1*, 23–40. 16

Lapusta, N., and Y. Liu (2009), Three-dimensional boundary integral modeling of spontaneous earthquake sequences and aseismic slip, *J. Geophys. Res.*, *114*, B09,303. 21

Lasocki, S., V. G. Karakostas, and E. E. Papadimitriou (2009), Assessing the role of stress transfer on aftershock locations, *J. Geophys. Res.*, *114*, B11,304. 11

Lavallee, D. (2008), On the random nature of earthquake sources and ground motions: A unified theory, *Adv. Geophys.*, *50*, 427–461. 9

Lavallee, D., P. C. Liu, and R. J. Archuleta (2006), Stochastic model of heterogeneity in earthquake slip spatial distributions, *Geophys. J. Int.*, *165*, 622–640. 9

Linker, M. F., and J. H. Dieterich (1992), Effects of variable normal stress on rock friction - observations and constitutive-equations, *J. Geophys. Res.*, *97*(B4), 4923–4940. 13

Mai, P. M., and G. C. Beroza (2002), A spatial random field model to charaterize complexity in earthquake slip, *J. Geophys. Res.*, *107*, 2308, doi:10.1029/2001JB000588. 9

Mallmann, E. P., and M. D. Zoback (2007), Assessing elastic Coulomb stress transfer models using seismicity rates in southern California and south-western Japan, *J. Geophys. Res.*, *112*, B03,304. 11

Marsan, D. (2003), Triggering of seismicity at short timescales following Californian earthquakes, *J. Geophys. Res.*, *108*(B5), 2266. 11

Marsan, D. (2005), The role of small earthquakes in redistributing crustal elastic stress, *Geophys. J. Int.*, *163*(1), 141–151, doi:10.1111/j.1365-246X.2005.02700.x. 10, 11

Marsan, D. (2006), Can coseismic stress variability suppress seismicity shadows? Insights from a rate-and-state friction model, *J. Geophys. Res.*, *111*, B06,305, doi:10.1029/2005JB004060. 7, 18

Marsan, D., and G. Daniel (2007), Measuring the heterogeneity of the coseismic stress change following the 1999 Mw7.6 Chi-Chi earthquake, *J. Geophys. Res.*, *112*, B07,305, doi:10.1029/2006JB004651. 18, 19, 20

Marsan, D., and S. S. Nalbant (2005), Methods for measuring seismicity rate changes: A review and a study of how the M-w 7.3 Landers earthquake affected the aftershock sequence of the M-w 6.1 Joshua Tree earthquake, *Pageoph*, *162*(6-7), 1151–1185. 11

McCloskey, J., S. S. Nalbant, S. Steacy, C. Nostro, O. Scotti, and D. Baumont (2003), Structural constraints on the spatial distribution of aftershocks, *Geophys. Res. Lett.*, *30*(12), 1610. 7, 8

McCloskey, J., S. S. Nalbant, and S. Steacy (2005), Indonesian earthquake: Earthquake risk from co-seismic stress, *Nature*, *434*(7031), 291. 4

Nalbant, S. S., A. Hubert, and G. C. P. King (1998), Stress coupling between earthquakes in northwest turkey and the north aegean sea, *J. Geophys. Res.*, *103*, 24,469–24,486. 3

Nalbant, S. S., J. McCloskey, S. S. Nalbant, and A. A. Barka (2002), Stress accumulation and increased seismic risk in eastern Turkey, *Earth Plan. Science Lett.*, *195*(3-4), 291–298. 7

Nostro, C., L. Chiaraluce, M. Cocco, D. Baumont, and O. Scotti (2005), Coulomb stress changes caused by repeated normal faulting earthquakes during the 1997 Umbria-Marche (central Italy) seismic sequence, *J. Geophys. Res.*, *110*(B5), B05S20. 8

Ogata, Y. (1998), Space-time point-process models for earthquake occurrences, *Ann. Inst. Stat. Math.*, *5*(2), 379–402. 17

Parsons, T. (2002), Global Omori law decay of triggered earthquakes: Large aftershocks outside the classical aftershock zone, *J. Geophys. Res.*, *107*, 2199. 11

Parsons, T., S. Toda, R. S. Stein, A. Barka, and J. H. Dieterich (2000), Heightened odds of large earthquakes near Istanbul: An interaction-based probability calculation, *Science*, *288*, 661–665. 4

Scholz, C. H. (1998), Earthquakes and friction laws, *Nature*, *391*, 37–42. 12

Sornette, D., and M. J. Werner (2005), Apparent clustering and apparent background earthquakes biased by undetected seismicity, *J. Geophys. Res.*, *110*(B9), B09,303. 11

Steacy, S., D. Marsan, S. S. Nalbant, and J. McCloskey (2004), Sensitivity of static stress calculations to the earthquake slip distribution, *J. Geophys. Res.*, *109*(B4), B04,303. 7, 11

Steacy, S., J. Gomberg, and M. Cocco (2005a), Introduction to special section: Stress transfer, earthquake triggering, and time-dependent seismic hazard, *J. Geophys. Res.*, *110*(B5), B05S01. 3, 6

Steacy, S., S. S. Nalbant, J. McCloskey, C. Nostro, O. Scotti, and D. Baumont (2005b), Onto what planes should Coulomb stress perturbations be resolved?, *J. Geophys. Res.*, *110*(B5), B05S15. 7

Stein, R. S. (1999), The role of stress transfer in earthquake occurrence, *Nature*, *402*(6762), 605–609. 12, 15

Stein, R. S., G. C. P. King, and J. Lin (1992), Change in failure stress on the southern san andreas fault system caused by the 1992 magnitude = 7.4 landers earthquake, *Science*, *258*, 1328–1332. 3

Stein, R. S., A. A. Barka, and J. H. Dieterich (1997), Progressive failure on the Northen Anatolian fault since 1939 by earthquake stress triggering, *Geophys. J. Int.*, *128*(3), 594–604. 3

Toda, S., R. S. Stein, P. A. Reasenberg, J. H. Dieterich, and A. Yoshida (1998), Stress transferred by the 1995, m_w=6.9 Kobe, Japan, shock: Effect on aftershocks and future earthquake probabilities, *J. Geophys. Res.*, *103*(B10), 24,543–24,565. 15, 16

Toda, S., R. S. Stein, and T. Sagiya (2002), Evidence from the AD 2000 Izu islands earthquake swarm that stressing rate governs seismicity, *Nature*, *419*(6902), 58–61. 15, 16

Toda, S., R. S. Stein, K. Richards-Dinger, and S. B. Bozkurt (2005), Forecasting the evolution of seismicity in southern California: Animations built on earthquake stress transfer, *J. Geophys. Res.*, *110*(B5), B05S16. 21

Wald, D. J., and T. H. Heaton (1994), Spatial and temporal distribution of slip for the 1992 Landers, California, earthquake, *Bull. Seis. Soc. Am.*, *84*(3), 668–691. 5

Ziv, A., and A. M. Rubin (2003), Implications of rate-and-state friction for properties of aftershock sequences: Quasi-static inherently discrete simulations, *J. Geophys. Res.*, *108*(B1), 2051. 21

Ziv, A., A. M. Rubin, and D. Kilb (2003), Spatiotemporal analyses of earthquake productivity and size distribution: Observations and simulations, *Bull. Seis. Soc. Am.*, *93*(3), 2069–2081. 14